Journal of Applied Polymer Science

Grafting Polymerization of Polylactic Acid on the Surface of Nano-SiO_2 and Properties of PLA/PLA-Grafted-SiO_2 Nanocomposites

Feng Wu, Xiaorong Lan, Deyun Ji, Zhengying Liu, Wei Yang, Mingbo Yang

College of Polymer Science and Engineering, State Key Laboratory of Polymer Materials Engineering,Sichuan University, Chengdu, Sichuan 610065, China

Correspondence to: M. Yang (E-mail: yangmb@scu.edu.cn)

ABSTRACT: Poly(lactic acid) (PLA) chains are directly grafted onto a silicon surface by *in situ* amidation and PLA/PLA-grafted SiO_2 nanocomposites are compounded using a Haake torque rheometer. To have a better understanding of the interaction between grafted polymer chains and PLA matrix, thermal, and rheological properties of PLA/PLA-grafted SiO_2 nanocomposites are explored. DSC analysis shows that PLA-grafted-SiO_2 can accelerate the cold crystallization rate and increase the degree of crystallinity of PLA. Shear rheology testing indicates that PLA/PLA-grafted-SiO_2 nanocomposites still exhibits the typical homopolymer-like terminal behavior at low frequency range even at a content of PLA-grafted-SiO_2 of 5 wt %, compared to PLA/SiO_2, it is also found that the nanocomposites show stronger shear-thinning behaviors in the high frequency region after grafting. In addition, elongation viscosity testing shows the entanglement between grafted chains and matrix that is needed to improve the melt strength of PLA. © 2013 Wiley Periodicals, Inc. J. Appl. Polym. Sci. 129: 3019–3027, 2013

KEYWORDS: biodegradable; grafting; nanoparticles; nanowires and nanocrystals; synthesis and processing

Received 12 July 2012; accepted 13 September 2012; published online 18 February 2013

DOI: 10.1002/app.38585

INTRODUCTION

Polylactide (PLA), as one of most popular bio-based and eco-friendly materials, has caused a wide range of research interests in recent decades.[1] Because of some excellent properties such as outstanding processing performance, high mechanical properties and excellent transparency,[2] PLA holds enormous potential as an alternative to the ubiquitous petroleum-based materials. Although PLA retains many advantages, the main drawbacks of the inherent brittleness, low melt strength, and slow crystallization rate, for instance, still limit its use in the field of daily necessities such as packaging and plastic bag. So many researches on the modification of PLA have been taken out, for example, melt blending with some ductile materials like PBS,[3] PBAT,[4] TPU Elastomer,[5] and LDPE,[6] grafting or blocking modification,[7,8] and adding some fillers such as nanoparticles[9–11] or nature fiber.[12]

In the aforementioned modification, with developments in nanoscience and nanoengineering fields, filling the nanoparticles into PLA has been a point of great interest to both industry and academy because the filled nanocomposites show some special properties such as improved thermal stability and remarkable electrical properties.[13] So many researches confirm that this is an effective way to enhance the performance of PLA. For example, Marius Murariu et al. prepare PLA films and fibers with PLA/ZnO composites.[14] Properties of PLA/organoclay,[15–18] PLA/TiO_2,[19,20] PLA/MWCNT[21–24] nanocomposites are also studied. Also base on hyperbranched polymer (HBP) nanostructure, PLA/HBP nanocomposites are prepared by Amar K. Mohanty[10] and the inherent brittleness of PLA has been modified. In nanoparticles modifications, SiO_2 nanoparticles which have larger specific surface, smaller particle size and higher density of silanol groups (Si—OH) on the surface are widely used and being a perfect candidate to improve the properties of polymers, including PLA.[25–28]

From the previous studies, we can see that the development of nanoscale dispersion of nanoparticles in polymer matrix and enhancing the interfacial interaction of nanoparticles/matrix are still two crucial problems existed in polymer nanocomposites,[29] and there are many researches[30–32] committing to solve these problems, the main method is the surface modification of nanoparticles. Except for silane modification, polymer grafting is one effective way in the nanoparticles modification. For nanocomposites modification, "grafting from" and "grafting to" are two ways to modify the nanoparticles in the studies springing up these years. Typically, "grafting from" method is used more widely because it is showed higher bonding density than

© 2013 Wiley Periodicals, Inc.

"grafting to" which involved the steric hindrance of polymer chains in the grafting step. But it might be difficult for "grafting from" method to control over the molecular weight and architecture of grafting polymers,[32] In contrast, "grafting to" is a modular approach in which polymers can be prepared prior to the grafting step, but the molecular weight of grafting polymers is often not high enough, e.g., PLA which M_n was 30,000 g mol^{-1} has been grafted.[33]

There are many researches about the modification of nanoparticles with PLA chains using either "grafting to" or "grafting from" method. Zhongkui Hong et al.[34,35] prepares the PLLA surface-grafted HAP nanoparticles by ring-opening polymerization of L-lactide (LLA) and further blended with PLLA. In Shifeng Yan[25]'s research, L-lactic acid oligomer is grafted to SiO_2 through condensation reaction without catalyst, and the results show that the grafted modification SiO_2 can serve as a candidate filler for toughing PLA. Ring-opening polymerization of L-lactide from silicon surface,[36] *in situ* melt polycondensation of L-lactic acid and surface-hydroxylated MgO,[37] PLA-grafted CNT,[38] and PLA-grafted TiO_2[39] are also prepared by "grafting from" method. In this study, we firstly prepare PLA-grafted-SiO_2 nanocomposites using an efficient "grafting to" method through the amidation reaction and the M_n of grafted PLA is 80,000 g mol^{-1}. And then we pay more attention to the final properties of PLA nanocomposites filled with the PLA-grafted-SiO_2. So the crystalline behavior and rheology properties of PLA/SiO_2 nanocomposites with and without grafting PLA are researched and compared.

EXPERIMENTAL

Materials

PLA_1 (M_w = 10.52e+4 g mol^{-1}, ρ = 1.24 g/cm^3), the commercial name of REVODE101 from Zhejiang Haizheng, China, was used as polymer matrix in this study. PLA_2 (M_w = 8.0e+4 g mol^{-1}, ρ = 1.24 g/cm^3, without end-blocking) for reaction in powder state was purchased from Shenzhen YiSheng, China. Fumed Silica named Aerosil 200 (hydrophilic) was provided by Zhoushan–Mingri, China. The SiO_2 showed spherical shape with a large surface area ($\geq$200 m^2 g^{-1}) and an average particle size of ~12 nm. The silanol group content was 1.37 $mmolg^{-1}$ by volumetrically measuring. The 3-aminopropyltriethoxysilane (APS; KH 550) (provided by Best-reagent company, Chengdu, China), dichloromethane (CH_2Cl_2) were used without further purification. *N,N*-dimethylformamide (DMF), toluene, and tetrahydrofuran (THF) were dried over 4A molecular sieves and distilled before used.

Functionalization of SiO_2 by *In Situ* Amidation Reaction with PLA_2

To change the surface property of SiO_2, PLA chains were grafted onto the SiO_2 nanoparticles directly through solution amidation reaction by *N,N′*-dicyclohexylcarbodiimide mediated. The grafting reaction was introduced by repeating two processes involving (Scheme 1): (1) aminopropyl triethoxysilane was fixed on the surface of virgin silicon; (2) PLA was introduced onto silicon surface which amino group as an initiator site.

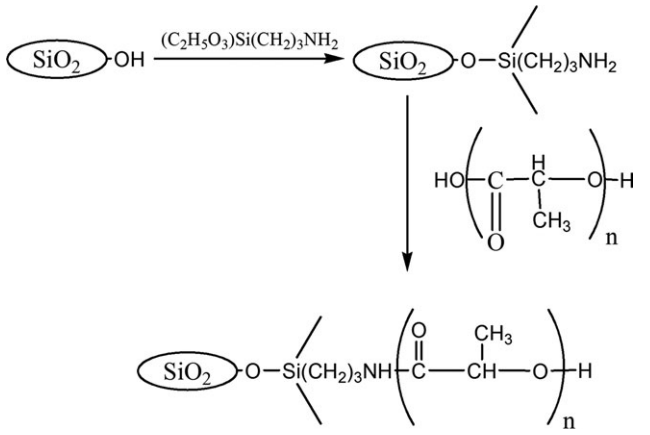

Scheme 1. Illustration of the grafting of PLLA onto APS-functionalized silica surface.

Introduction of Amino Groups onto Silicon Surface. The typical example of introduction of amino groups onto silicon surface is as follows[40]: 4 g SiO_2 were dispersed in a three-necked flask with 100 mL toluene, after ultrasonic processing for 120 min at room temperature, a solution of APS (10 mL)/dry toluene (50 mL) was added dropwise under nitrogen protecting. Follow up treatment for 240 min at 80°C in ultrasonic environment under nitrogen, the flask was sealed into an oil bath and refluxed for 180 min. After cooling to room temperature, the nanoparticles modified by KH550 was suction filtered and washed with toluene, then extracted with toluene in a Soxhlet apparatus for 8 hr to remove the residual APS. The functionalized silicon was dried *in vacuo* at 60°C for 36 h, weighed, recorded as SiO_2—NH_2 and stored for future use.

Grafting of PLA onto Silica Nanoparticles. The amidation reaction carried out as follows. After ultrasonic processing for 120 min, the dried SiO_2—NH_2 (4 g)/dry DMF (100 mL) suspension was added into PLA (25 g)/dry DMF (150 mL) solution. Then 1780 mg DCC and 520 mg DMAP were added into the mixture charged in a flask. Followed by ultrasonic processing for 150 min at 36°C, the flask was sealed into an oil bath and refluxed for 6 h. All operation was carried out under nitrogen. After that, the reaction mixture was separated by centrifugation for 45 min at 8000 rpm. The centrifugation procedure was as follows: The products were washed with CH_2Cl_2 after centrifugalized for 15 min, and then the aforementioned procedure was repeated for three times. Ultimately the product was purified by Soxhlet extraction for 50 h with hot THF to remove the *N,N′*-dicyclohexylurea (DCU) and unbound PLA from the particles. The final product was dried *in vacuo* at 60°C for 72 h, weighed, recorded as PLA-*g*-SiO_2 and stored for future use.

Preparation of PLA/PLA-*g*-SiO_2 Nanocomposites

PLA nanocomposites were prepared in the Haake torque rheometer (XSS-300, Shanghai Kechuang Rubber Plastics Machinery Set, Shanghai, China). PLA_1 and PLA-*g*-SiO_2 both were dried *in vacuo* at 60°C for 12 h before melt blending. The mixture of PLA_1 and PLA-*g*-SiO_2 were premixed at 175°C and the blade rotated at a constant rate of 50 rpm for 5 min. The samples with 0.3, 0.5, 1.0, 2.0, 3.0, and 5.0 wt % PLA-*g*-SiO_2 were

prepared and labeled as PLA-*g*-0.3, PLA-*g*-0.5, PLA-*g*-1, PLA-*g*-2, PLA-*g*-3, PLA-*g*-5 nanocomposites. The neat PLA_1 was subjected to the mixing treatment so as to have the same thermal history as the blends. At the same time, PLA/SiO_2 nanocomposites (defined as PLA-0.3, PLA-0.5, PLA-1, PLA-2, PLA-3, and PLA-5) were also prepared in the same way for comparison.

Testing and Characterization

The FTIR analysis was performed on a Nicolet 6700 FTIR spectrometer in the transmission mode at the wavelength range of 400–4000 cm^{-1} with the resolution of 4 cm^{-1}. Samples of ungrafted SiO_2, SiO_2—NH_2 and PLA grafted SiO_2 particles were respectively mixed with KBr powders and pressed into a disk for IR measurement.

For supplementary confirming the grafted PLA and calculating the amount of amino groups and PLA introduced onto the silicon surface, TGA data were obtained between 150 and 700°C. The resulting TGA signal was obtained by a thermobalance (TGA Q600, TA Instruments, USA) apparatus from 30 to 700°C at a heating rate of 10°C min^{-1} under nitrogen atmosphere.

The crystallization behaviors of PLA/PLA-*g*-SiO_2 and PLA/SiO_2 nanocomposites were studied by differential scanning calorimeter (DSC) (Q20, TA Instruments, New Castle, DE). Samples of about 5 mg were dried *in vacuo* at 60°C for 24 h, and then inserted into aluminum pans for scanning as follows: the test samples were heated to 200°C at a rapid rate and kept for 5 min to eliminate the thermal history, then cooled to 20°C at 10°C min^{-1} and held at 20°C for 3 min, they were then reheated to 200°C at rate of 10°C min^{-1}. The cooling and the second heating curves were recorded to describe the crystallization and melting behaviors of the nanocomposites. And the crystallinity X_c was calculated as follow:

$$X_C(\%) = 100(\Delta H_m/\Delta H_f)$$

Where ΔH_m, melting enthalpy for sample obtained at second heating curve in DSC test

ΔH_f, 93.6 J g^{-1},[28] enthalpy of fusion for the perfectly crystalline PLA

The melt viscoelasticity of the PLA nanocomposites was examined using a stress-controlled rheometer (AR2000EX, TA Instruments, New Castle, DE) with parallel plate geometry. Samples for testing were compression molded into disks with a diameter of 25 mm and thickness of 2.0 mm at 10 MPa, 175°C. The frequency sweep from 0.01 to 100 Hz was conducted at 170°C with a strain of 2.0% (within the linear viscoelastic region of PLA determined from strain sweep experiment at a frequency of 1 Hz) and a gap of 1200 μm under nitrogen to protecting PLA from degradation during test.

Extensional rheology of PLA nanocomposites at constant Hencky strain rate (ε_0) in the melt state was conducted with ARES extensional rheometer with the extensional viscosity fixture (EVF, TA Instruments, USA). The EVF design was based on the original Meissner concept to elongate the sample within a confined space by expelling the sample with rotary clamps. Instead of the rotary clamps, two cylinders were used to wind up the sample; one cylinder was rotating, the other measuring the tensile force exerted on the samples.[41] Before each run of the elongation test, samples with a size of 17 × 10 × 1 mm^3 were dried *in vacuo* at 60°C overnight. Testing Hencky strain rate (ε_0) was 0.1 s^{-1} and testing temperature was 153°C above the T_m (about 149°C) of PLA.

RESULTS AND DISCUSSION

Surface Grafting of SiO_2 Nanoparticles

Figure 1(A) shows the FTIR spectra of SiO_2—NH_2 and PLA-*g*-SiO_2 synthesized as mentioned above. Stretching bands at 406, 865, 1100 cm^{-1} which corresponds to the typical Si—O—Si structure existed in FTIR spectrum of all three samples. Compared with the FTIR spectra of SiO_2 and SiO_2—NH_2, new absorption peaks appear at 1760 cm^{-1} for the PLA-*g*-SiO_2 which corresponding to the typical carbonyl stretching absorption of PLA grafted on the SiO_2 nanoparticles.[42] Also from Figure 1(B), an absorption peak still appears at 2942.48 cm^{-1} for SiO_2—NH_2 which corresponding to the CH bonds vibration of KH550 grafted on the SiO_2 nanoparticles, compared to the spectral of SiO_2—NH_2, not only new absorption peak appears at 2942.48, 2994.28 cm^{-1} for the PLA-*g*-SiO_2 results from the stretching vibration of CH bonds vibration of the CH_2 and CH_3 groups of PLA, but also a new peak appears at 1490 cm^{-1} for the PLA-*g*-SiO_2 results from the bending vibration of CH bonds of PLA. Further, to confirm the amidation reaction, we enlarge the FTIR spectra of PLA-*g*-SiO_2 and SiO_2—NH_2 in the scale of 300 to 2000 cm^{-1} [seen in Figure 1(B)]. It is more clearly that after PLA grafted on SiO_2, the characteristic band at 1637 cm^{-1} which attributed to the amino group of APS introduced onto the silicon surface shifts to 1651 cm^{-1}, showing the transformation from amide band II(δ_{N-H}) to amide band I($\nu_{C=O}$). In other words, the peak shift confirms the formation of amide bond through solution amidation reaction of PLA with SiO_2—NH_2 by *N,N′*-dicyclohexylcarbodiimide mediated. As for the C—O stretching band which should exist at 1182, 1128, and 1090 cm^{-1}, we think Si—O—Si stretching band at 1100 cm^{-1} has covered them. So FTIR results indicate that PLA chains have been successfully grafted onto SiO_2 nanoparticles surface in this way.

The PLA-grafted SiO_2 is complementally confirmed by TGA thermograms, and the percentage of grafting of final products is also calculated. So Figure 2(A) shows the TGA diagrams of SiO_2, SiO_2—NH_2, PLA-*g*-SiO_2, and the TGA thermograms of pure PLA_2 is showed in Figure 2(B). It is generally considered that the small weight losses between 40 and 150°C are mainly due to the dehydration process of adhesive water and crystal water on the surface of SiO_2. So the desorption of hydroxyl on the surface of SiO_2 nanoparticles is thought to be heated to 150°C or higher. So we calculate the percentage of grafting base on the weight loss between 150 and 800°C. In Figure 2(A), the desorption of the surface functional groups of silanized SiO_2 (SiO_2—NH_2) is carried out mainly from 400 to 600°C. The temperature of maximum speed on loss in weight is 499.96°C, which is well consistent with the research report of Jian Yu.[40] And the weight loss of SiO_2—NH_2 is 10.75% getting from the curve. When PLA chains are introduced onto the surface of SiO_2, the thermal desorption of the PLA-*g*-SiO_2 could be divided into two stages. One stage is from 250 to 375°C and the

Applied Polymer SCIENCE

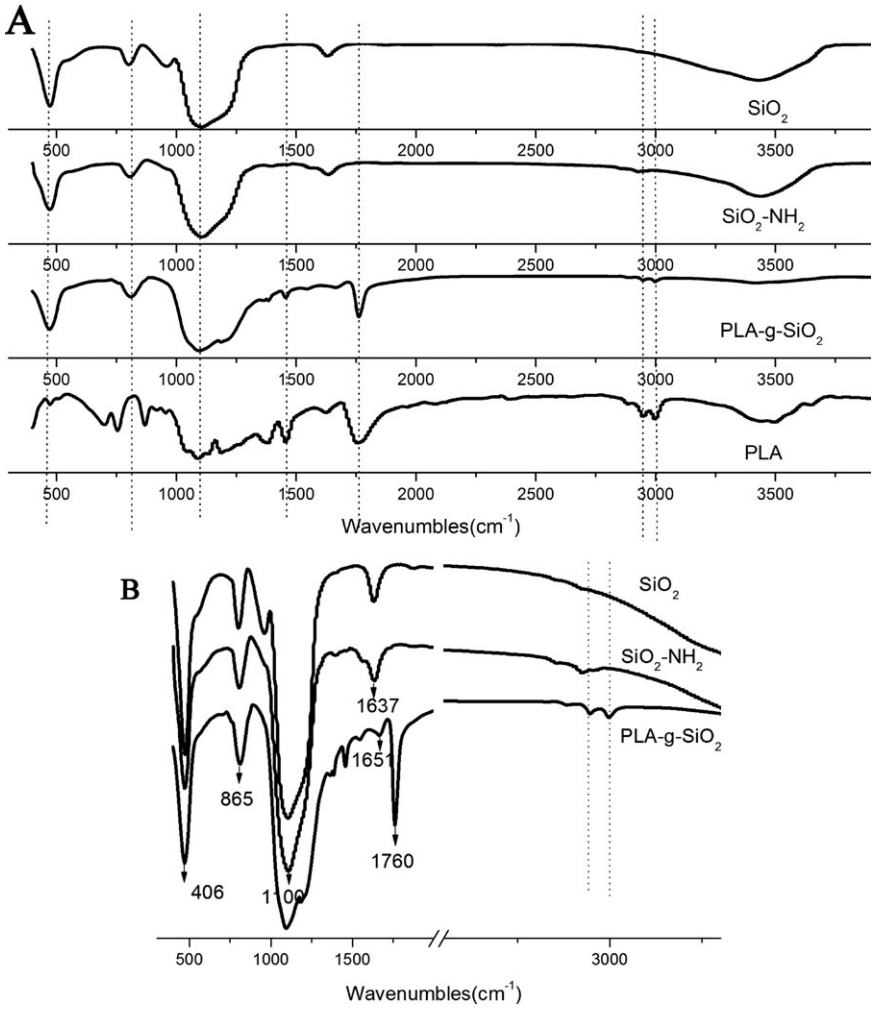

Figure 1. FTIR spectra of SiO_2, SiO_2—NH_2, PLA-*g*-SiO2, and PLA_2: (A) 300–3900 cm^{-1} and (B) 300–3300 cm^{-1} region which break from 2000 to 2550 cm^{-1}.

temperature of maximum speed on loss in weight is 303.86°C, the temperature range of second degradation stage is from 400 to 575°C and the maximum degradation temperature was 428.77°C. These two stages consist of the thermal decomposition of PLA and KH550 grafted on the surface of SiO_2. Compared to the TGA results of pure PLA show in Figure 2(B), the degradation temperature range of PLA grafted on the surface of SiO_2 is higher than pure PLA. The results indicate that the thermal stability of PLA has been increased after grafted onto SiO_2.

According to the TGA results, we also can roughly calculate the amount of PLA grafted onto the SiO_2 surface as follow formulas and the data are summarized in Table I. The results indicate that as more as 15.23 wt % PLA is successfully grafted.

$$\text{Overallgrafting}(\%) = \frac{\text{OverallOrganicComposition/g}}{\text{virginSiO}_2\text{/g}} \times 100$$

Net grafting (%) = Overall grafting (%)-Silane grafting (%)

The results were calculated base on the weight loss obtained between 150 and 700°C, thus, PLA grafting was 15.23 wt %, corresponding to 0.38 $mmolg^{-1}$ (PLA-grafted-SiO_2).

The FTIR and TGA results further prove that PLA chains are chemically linked onto the silicon surface. Hence, good compatibility is expected between the PLA-*g*-SiO_2 and PLA matrix. So PLA/SiO_2-*g*-PLA nanocomposites are prepared and the properties of them are investigated.

Properties of PLA/SiO_2-*g*-PLA Nanocomposites

The Thermal Properties of PLA Nanocomposites. The crystallization behavior of PLA nanocomposites was studied by DSC and the results were shown in Figure 3. Because of the relatively low crystallization rate,[43] PLA showed no crystallization peak at a cooling rate of 10°C min^{-1} in this study. Figure 3(A) showed the DSC cooling scans of PLA/PLA-*g*-SiO_2 nanocomposites after erasing previous thermal history in Figure 3(A). Unlike PLA/SiO_2 nanocomposites without melt crystallization peak, with the increasing of PLA-*g*-SiO_2 content, it was notable that a weak crystallization peak appeared around 115°C when the content of PLA-*g*-SiO_2 reached 5 wt %. It seemed that PLA-*g*-SiO_2 could accelerate the crystallization rate of PLA as a nucleating agent. This was more obvious in nonisothermal cold crystallization process of PLA nanocomposites [Figure 2(B, D)]. A cold

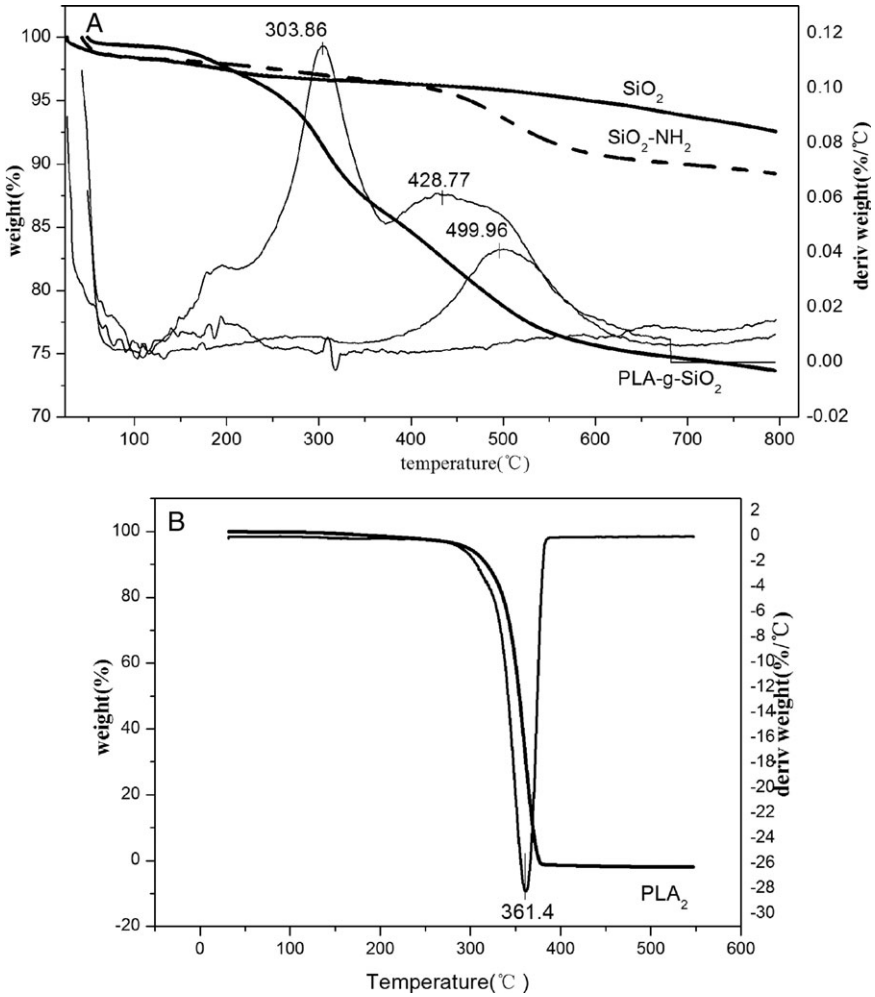

Figure 2. TG and DTA curves of SiO_2, SiO_2—NH_2, PLA-*g*-SiO_2 (A) and pure PLA_2 (B).

crystallization peak would appear at the heating rate of 10°C min^{-1} also due to the relatively low crystallization rate, and for PLA/SiO_2 nanocomposites, virgin SiO_2 nanoparticles did not show any effect on the cold crystallization behavior of PLA when the addition amount of SiO_2 achieving as 5 wt %, as showed in Figure 3(D). The cold crystallization temperature for all samples was listed in Table II. Different from PLA/SiO_2 nanocomposites, combined with the second heating curve in Figure 3(B), the cold crystallization temperature of PLA tended to move to low temperature range with the increasing of PLA-*g*-SiO_2 content showed in Figure 3(B), even the content of PLA-*g*-SiO_2 achieving as 5 wt %, the cold crystallization temperature was 119.19, 6°C lower than the temperature of neat PLA. And the crystallinity X_c of PLA/PLA-*g*-SiO_2 nanocomposites changed notably, the crystallinity of PLA-*g*-5 achieved as high as 26.84%, notably higher that PLA-5.

Table I. The Overall and Net Grafting of SiO_2, SiO_2—NH_2, SiO_2—PLA

Materials	Overall grafting (wt)	Net grafting (wt)
SiO_2	5.39%	
SiO_2—NH_2	8.95%	3.64%
PLA-*g*-SiO_2	24.18%	15.23%

The grafting PLA chains would be an important factor on the different crystallization behavior of PLA nanocomposites. And this difference illustrated that the initial cold crystallization ability of PLA slightly improved with the increasing of PLA-*g*-SiO_2 content.

It was obvious that the functioned silicon nanoparticles acted more active in promoting the crystallization of PLA than bare SiO_2. From the DSC scans of typical thermal behaviors of PLA/PLA-*g*-SiO_2 nanocomposites, glass transition (T_g), cold crystallization peak (T_c) and the melting point (T_m), were summarized in Table III. The introduction of PLA-*g*-SiO_2 into PLA did not result in a noticeable change in T_g (~61°C) and T_m (ca. 147°C) possibly due to the relatively low concentration of PLA-*g*-SiO_2 in composites. It was known that branched PLA chains could play a role of nucleating site on the crystallization of PLA,[44] from the analysis above, we thought that the grafting PLA chains on the surface of SiO_2 nanoparticles promoted the melt and cold crystallization of PLA in some degree as nucleating sites. And this was under investigation by us.

The Melt Rheology Properties of PLA Nanocomposites

Dynamic oscillatory shear measurements. Generally, dynamic oscillatory shear measurements proved to be a useful tool to

Applied Polymer SCIENCE

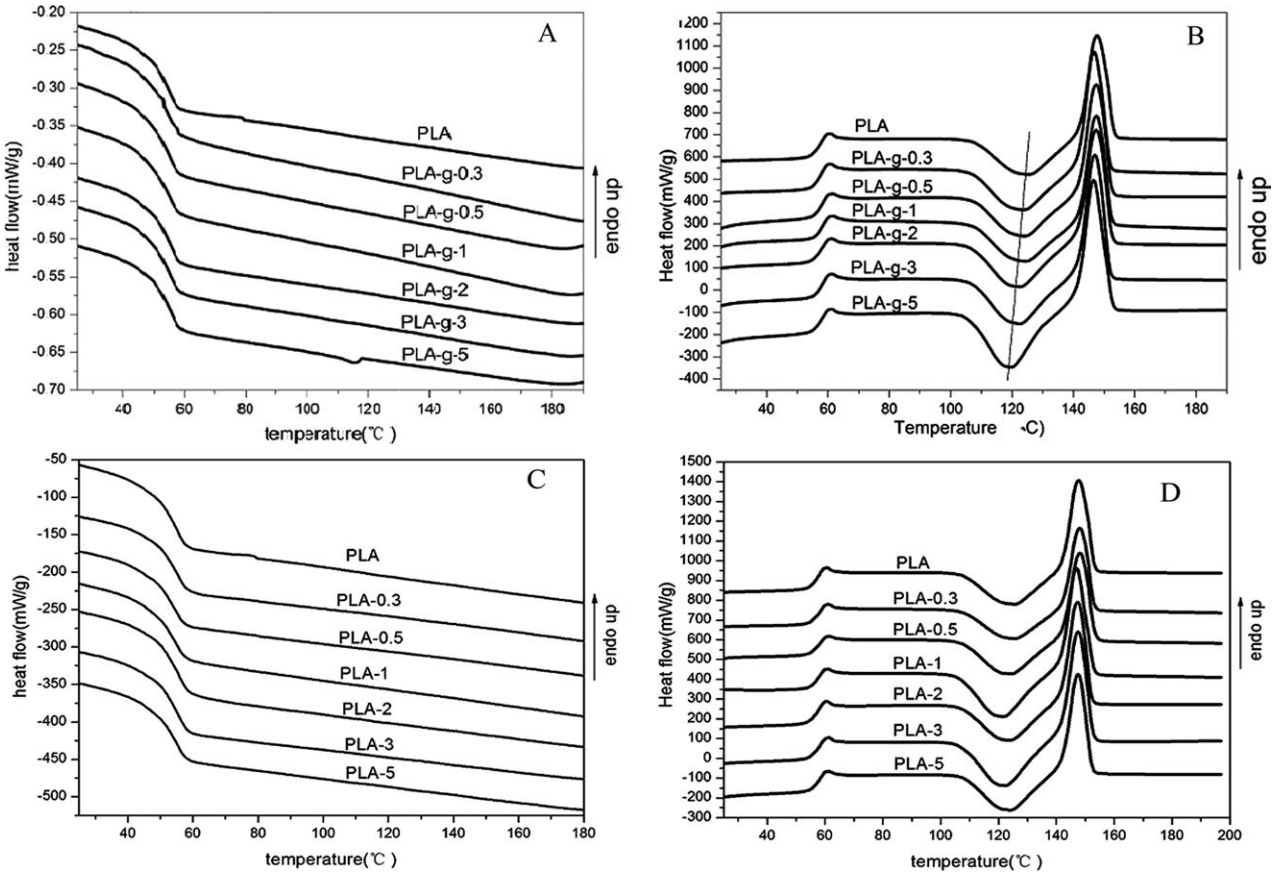

Figure 3. DSC traces of PLA nanocomposites at a cooling rate of 10°C min^{-1} (left) and at a second heating rate of 10°C min^{-1} (right): PLA/PLA-*g*-SiO_2 (A and B), PLA/SiO_2 (C and D).

characterize the behavior of nanofiller network in polymer matrix.[45] So the storage moduli and loss moduli at different loadings for PLA/SiO_2 and PLA/PLA-*g*-SiO_2 nanocomposites obtained from dynamic rheology measurements were illustrated in Figures 4 and 5, respectively. In the case of PLA samples, it was excepted that typical homopolymer-like terminal behavior (at low frequencies, PLA chains were fully relaxed and exhibited typical homopolymer-like terminal behavior with scaling properties of $\sim G' \sim \omega^2$ and $G'' \sim \omega$ as shown in Figure 4) exhibited at low frequency. After nanosilicon was added, we could see that, the storage moduli G' was higher than loss moduli G'' at low frequency when the SiO_2 loadings achieving up to 3 wt % and above. And at higher SiO_2 loading (5 wt %), the dependence of G' on frequency was weak and G'' was totally independent of the frequency at low frequency range, exhibiting nonterminal low frequency behavior. It was generally accepted that in dynamic oscillatory shear measurements, the characterization of solid-like behavior in nanocomposites was mainly focusing on the low frequency range.[45] So this nonterminal low frequency behavior revealed that large agglomeration of nanoparticles formed in the samples, result in large-scale polymer relaxations in composites were effectively restrained. But for PLA/PLA-*g*-SiO_2 nanocomposites, we had the master curves for G' and G'' of PLA/PLA-*g*-SiO_2 composites illustrated in Figure 5, the same as other reports,[15,46] elastic modulus G' monotonously increased with the content of PLA-*g*-SiO_2 nanoparticles. But compared to

Table II. The T_g, T_c, T_m, and X_c (crystallinity) of PLA/SiO^2

Sample	T_g	T_c	T_m	X_c (%)
PLA	60.49	125.32	147.72	21.45
PLA-0.3	60.83	125.45	148.04	18.30
PLA-0.5	61.02	124.26	148.21	20.65
PLA-1	60.83	121.74	146.97	24.47
PLA-2	60.25	124.15	147.33	21.53
PLA-3	61.02	122.35	147.55	25.37
PLA-5	60.83	125.32	147.55	21.34

Table III. The T_g, T_c, T_m, and X_c (crystallinity) of PLA/PLA-*g*-SiO^2

Sample	T_g	T_c	T_m	X_c (%)
PLA	60.49	125.32	147.72	21.45
PLA-*g*-0.3	60.07	123.53	146.74	22.84
PLA-*g*-0.5	60.86	124.07	147.47	22.01
PLA-*g*-1	61.05	124.14	147.51	21.13
PLA-*g*-2	61.24	122.64	147.40	23.26
PLA-*g*-3	61.24	122.49	146.99	24.55
PLA-*g*-5	60.83	119.19	146.60	26.84

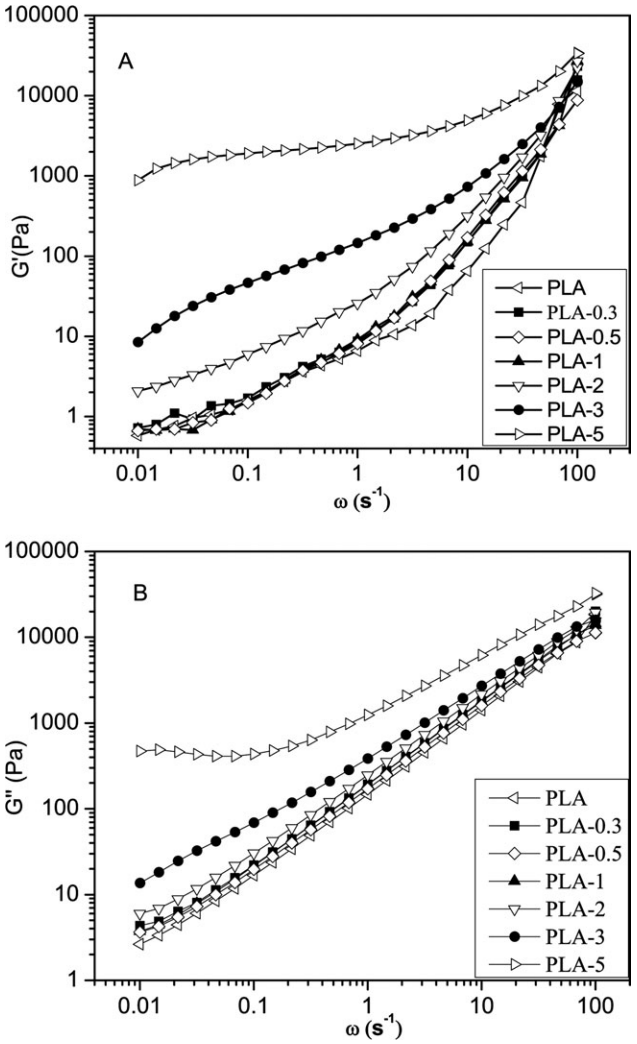

Figure 4. 170°C storage moduli (A) and loss moduli (B) at different loadings for PLA/SiO_2 nanocomposites.

PLA/SiO_2 composites, it was worth noting that the nanocomposites still exhibited the typical homopolymer-like terminal behavior at low frequency range even PLA-*g*-SiO_2 loading was as high as 3 wt % and above. The phenomenon which the transition from the solid-like behavior at lower frequencies to the matrix-dominated behavior at higher frequencies didn't happen indicated that the nanofiller network showed more stable in the range of whole frequency after grafted. Also the complex viscosities η^* of PLA nanocomposites showed difference after the nanoparticles was grafted from the analysis of follow part.

The complex viscosities η^* of PLA, PLA/SiO_2, and PLA/PLA-*g*-SiO_2 composites exhibited in Figure 6. Neat PLA performs Newtonian behavior in the high frequency as a semistiff polymer.[47] The complex viscosities η^* of PLA/SiO_2 composites was demonstrated in Figure 6(A), It is obvious that η^* increased with the increase of the SiO_2 content and this behavior is mainly dependence on the nanoparticles content. Along with the increase of the SiO_2 content, shear-thinning behaviors appeared. When the SiO_2 loading achieved as high as 5 wt %, strong shear-thinning behaviors were observed in the full frequency region. Similar rheological behaviors were observed in polymer nanocomposites containing clay OMMT.[48] But if silicon was grafted, different performance would exhibit. After PLA grafted on the SiO_2, we got that the complex viscosities η^* still increased continuously with the increase of PLA-*g*-SiO_2 content [Figure 6(B)], which is different from the result of Yan-Bing Luo's.[19] But unlike PLA/SiO_2 nanocomposites, the complex viscosities didn't change notably, it didn't exhibit a transition from liquid-like to solid-like viscoelastic behavior even at high PLA-*g*-SiO_2 loading (5 wt %). As discussed previously, it revealed that the grafted nanofiller dispersed more uniform in the matrix, and so the nanofiller network exhibited more stable under shearing.

Except for this, we found that more obvious shear-thinning behaviors happened in the high frequency region in Figure 6(B) for PLA-*g*-2 and PLA-*g*-3 nanocomposites. We thought that, for PLA-*g*-SiO_2/PLA blends, after grafted, the entanglements between grafted PLA chains and matrix molecular chains would make the nanoparticles network more perfect. So the molecular

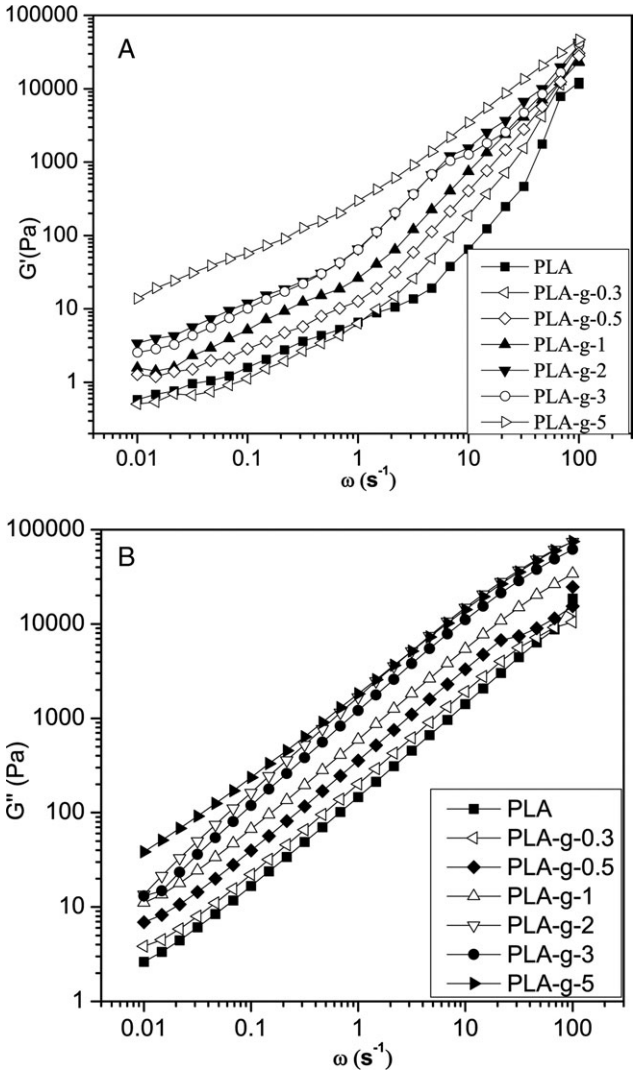

Figure 5. 170°C storage moduli (A) and loss moduli (B) at different loadings for PLA/PLA-*g*-SiO_2 nanocomposites.

Applied Polymer SCIENCE

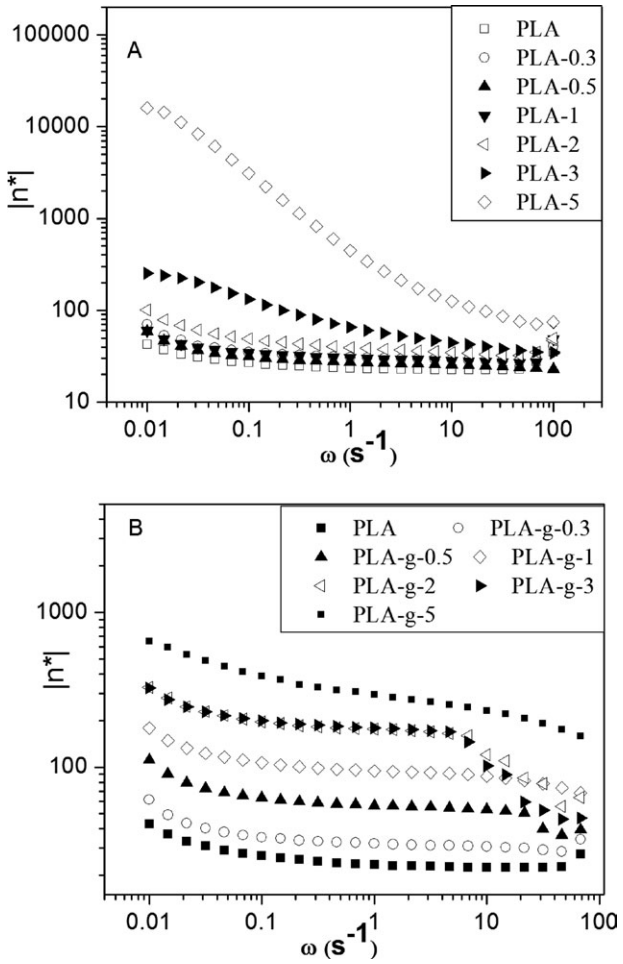

Figure 6. 170°C complex viscosity at different loadings for PLA/SiO_2 (A) and PLA/PLA-*g*-SiO_2 (B) nanocomposites.

disentanglement became more obvious under shearing, result to the ruin of nanocomposites network and so stronger shear-thinning behaviors exhibited in the high frequency region.

From the analysis above, we got that the distribution of grafted silicon nanoparticles in PLA matrix had been greatly improved. And the entanglement between grafted PLA chains and PLA matrix greatly improved the stable of nanofiller network. Finally the entanglement effect influenced the rheology properties of PLA greatly.

Elongational viscosity testing. The extensional rheology testing of nanocomposites was actualized at 153°C, and the constant Hencky strain rate (ε_0) was 0.1 s^{-1} and the results were showed in Figure 7. In the following discussion, data for pure PLA and the composites which loading silicon nanoparticles lower than 2 wt % didn't get because the sample sagged down as the low melt strength. We can't obtain the melt strength directly in the test, so using the tensile force as a comparable parameter to compare the melt strength of PLA nanocomposites with different nanoparticles loadings seemed like a viable way. Figure 7(A) exhibited the tensile force vs. time for PLA nanocomposites at 153°C. The peak value was defined as the melt strength of materials. From Figure 7(A), it could be obtained that the melt strength increased through adding nanoparticles to matrix. Especially for PLA-5 which large agglomeration of nanoparticles happened, the tensile force was further greater than others. But large agglomeration of nanoparticles was not expected in as it would adversely affect the properties of nanocomposites. The molecular entanglement effect in PLA/PLA-*g*-SiO_2 nanocomposites mentioned in shearing viscosity measurement was also conducted in elongational viscosity testing, which can be obtained from Figure 7(B) that illustrated the elongational viscosity vs. time for PLA nanocomposites. Compared to PLA/SiO_2 nanocomposites, the Extensional viscosities of PLA/PLA-*g*-SiO_2 tended to rising or maintain the same level after a certain time of stretching for PLA-*g*-5 and PLA-*g*-2 nanocomposites, seemed like a characterization of strain hardening. This demonstrated that the molecular entanglement between grafted PLA chains and PLA matrix provided the condition for obtained strain hardening of polymer melt in processing. Only nanoparticles played the role of the physical crosslinking points in the matrix, strain hardening expected to appear when the physical crosslinking network would suppress the contribution of stretching on molecular orientation along the flowing direction during the elongational flow. And this function is still under research for us.

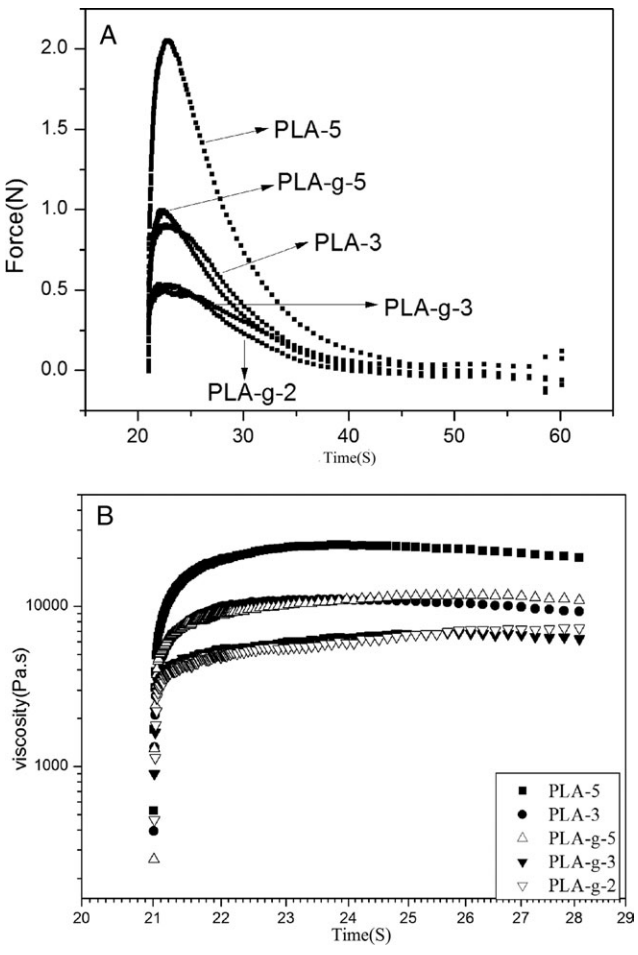

Figure 7. 153°C tensile force VS time (A) and viscosity VS time (B) for PLA/SiO_2 and PLA/PLA-*g*-SiO_2 nanocomposites (hencky strain = 0.1 s^{-1}).

CONCLUSION

Functionalization of SiO_2 nanoparticles with PLA chains was completed first, and then the reaction of PLA chains to the nanoparticles was confirmed by FTIR and TGA analysis. Also the amount of grafted PLA chains was calculated from TGA data and the net grafting was relatively high. DSC data showed that the introduction of PLA-*g*-SiO_2 into PLA matrix could improve the crystallinity of the composite slightly. Dynamic oscillatory shear measurements showed that the grafted silicon nanoparticles performed stronger shear-thinning behaviors. Even more interesting was the result from elongational viscosity testing, it exhibited the molecular condition for strain hardening, which is worth further research. We'd like to see the as-prepared PLA/PLA-*g*-SiO_2 nanocomposites could be a candidate for the fabrication of biomedical materials and eco-friendly daily products solving environmental problem.

ACKNOWLEDGMENTS

This research was supported by the National Natural Science Foundation of China (Grant No.51033003).

REFERENCES

1. Madhavan Nampoothiri, K.; Nair, N. R.; John, R. P. *Bioresour. Technol.* **2010,** *101*, 8493.
2. Williams, C.; Hillmyer, M. *Polym. Rev.* **2008,** *48*, 1.
3. Yokohara, T.; Okamoto, K.; Yamaguchi, M. *J. Appl. Polym. Sci.* **2010,** *117*, 2226.
4. Jiang, L.; Wolcott, M. P.; Zhang, J. *Biomacromolecules* **2005,** *7*, 199.
5. Han, J. J.; Huang, H. X. *J. Appl. Polym. Sci.* **2011,** *120*, 3217.
6. Anderson, K. S.; Lim, S. H.; Hillmyer, M. A., *J. App. Polym. Sci.* **2002**, *89*, 3757.
7. Cai, Q.; Zhao, Y.; Bei, J.; Xi, F.; Wang, S., *Biomacromolecules* **2003**, *4*, 828.
8. Wang, H.; Zhang, Y.; Tian, M.; Zhai, L.; Wei, Z.; Shi, T. *J. Appl. Polym. Sci.* **2008,** *110*, 3985.
9. Pilla, S.; Kramschuster, A.; Lee, J.; Clemons, C.; Gong, S.; Turng, L.-S. *J. Mater. Sci.* **2010,** *45*, 2732.
10. Bhardwaj, R.; Mohanty, A. K. *Biomacromolecules* **2007,** *8*, 2476.
11. Turan, D.; Sirin, H.; Ozkoc, G. *J. Appl. Polym. Sci.* **2011,** *121*, 1067.
12. Wong, S.; Shanks, R. A.; Hodzic, A. *Macromol. Mater. Eng.* **2004,** *289*, 447.
13. Ray, S. S.; Okamoto, M. *Macromol. Rapid Commun.* **2003,** *24*, 815.
14. Murariu, M.; Doumbia, A.; Bonnaud, L.; Dechief, A. L.; Paint, Y.; Ferreira, M.; Campagne, C.; Devaux, E.; Dubois, P. *Biomacromolecules* **2011,** *12*, 1762
15. Di, Y.; Iannace, S.; Maio, E. D.; Nicolais, L. *J. Polym. Sci. Part B: Polym. Phys.* **2005,** *43*, 689.
16. Svagan, A. J.; Åkesson, A.; Cárdenas, M.; Bulut, S.; Knudsen, J. C.; Risbo, J.; Plackett, D. *Biomacromolecules* **2012,** *13*, 397.
17. Lee, S.; Kim, C.-H.; Park, J.-K. *J. Appl. Polym. Sci.* **2006,** *101*, 1664.
18. Thellen, C.; Orroth, C.; Froio, D.; Ziegler, D.; Lucciarini, J.; Farrell, R.; Dsouza, N.; Ratto, J. *Polymer* **2005,** *46*, 11716.
19. Luo, Y.-B.; Li, W.-D.; Wang, X.-L.; Xu, D.-Y.; Wang, Y.-Z. *Acta Mater.* **2009,** *57*, 3182.
20. Nakayama, N.; Hayashi, T. *Polym. Degrad. Stabil.* **2007,** *92*, 1255.
21. Chrissafis, K. *Thermochim. Acta* **2010,** *511*, 163.
22. Xu, Z.; Niu, Y.; Wang, Z.; Li, H.; Yang, L.; Qiu, J.; Wang, H. *ACS Appl. Mater. Interfac.*, to appear.
23. Kuan, C.-F.; Chen, C.-H.; Kuan, H.-C.; Lin, K.-C.; Chiang, C.-L.; Peng, H.-C. *J. Phys. Chem. Solids* **2008,** *69*, 1399.
24. Yoon, J. T.; Lee, S. C.; Jeong, Y. G. *Compos. Sci. Technol.* **2010,** *70*, 776.
25. Yan, S.; Yin, J.; Yang, Y.; Dai, Z.; Ma, J.; Chen, X. *Polymer* **2007,** *48*, 1688.
26. Wu, L.; Cao, D.; Huang, Y.; Li, B.-G. *Polymer* **2008,** *49*, 742.
27. Huang, T. C.; Yeh, J. M.; Yang, J. C. *Adv. Mater. Res.* **2010,** *123*, 1215.
28. Huang, J.-W.; Chang Hung, Y.; Wen, Y.-L.; Kang, C.-C.; Yeh, M.-Y. *J. Appl. Polym. Sci.* **2009,** *112*, 3149.
29. Giannelis, E. P. *Adv. Mater.* **2005,** *17*, 525.
30. Glogowski, E.; Tangirala, R.; Russell, T. P.; Emrick, T. *J. Polym. Sci. Part A: Polym. Chem.* **2006,** *44*, 5076.
31. Zhou, T.; Ruan, W.; Mai, Y.; Rong, M.; Zhang, M. *Compos. Sci. Technol.* **2008,** *68*, 2858.
32. Xie, L.; Xu, F.; Qiu, F.; Lu, H.; Yang, Y. *Macromolecules* **2007,** *40*, 3296.
33. Lou, X.; Detrembleur, C.; Sciannamea, V.; Pagnoulle, C.; Jérôme, R. *Polymer* **2004,** *45*, 6097.
34. Hong, Z.; Qiu, X.; Sun, J.; Deng, M.; Chen, X.; Jing, X. *Polymer* **2004,** *45*, 6699.
35. Hong, Z.; Zhang, P.; He, C.; Qiu, X.; Liu, A.; Chen, L.; Chen, X.; Jing, X. *Biomaterials* **2005,** *26*, 6296.
36. Joubert, M.; Delaite, C.; Bourgeat-Lami, E.; Dumas, P. *J. Polym. Sci. A Polym. Chem.* **2004, 42, 1976.**
37. Li, Y. H.; Sun, X. S. *Biomacromolecules* **2010, 11, 1847.**
38. Olalde, B.; Aizpurua, J. S. M.; Jurado, M. A. J. *J. Phys. Chem. C* **2008,** *112*, 10663.
39. Luo, Y.-B.; Wang, X.-L.; Xu, D.-Y.; Wang, Y.-Z. *Appl. Surf. Sci.* **2009,** *255*, 6795.
40. Guo, Z.-X.; Yu, J. *J. Mater. Chem.* **2002,** *12*, 468.
41. Inc, R. S., ARES Operator's Manual; TA Instruments Waters LLC, USA, 2006.
42. Li, Y.; Chen, C.; Li, J.; Sun, X. S. *Polymer*, to appear.
43. Li, H.; Huneault, M. A. *Polymer* **2007,** *48*, 6855.
44. Nofar, M.; Zhu, W.; Park, C. B.; Randall, J. *Indus. Eng. Chem. Res.* **2011,** *50*, 13789.
45. Block, C.; Watzeels, N.; Rahier, H.; Mele, B. V.; Assche, G. V. *J. Therm. Anal. Calorim.* **2011,** *105*, 731.
46. Sinha Ray, S.; Okamoto, M. *Macromol. Mater. Eng.* **2003,** *288*, 936.
47. Dorgana, J. R.; Williams, J. S. *J. Rheol.* **1999,** *43*, 1141.
48. Wang, B.; Wan, T.; Zeng, W. *J. Appl. Polym. Sci.* **2011,** *121*, 1032.